



Natural Resources
Canada

Ressources naturelles
Canada



Contrasting metamorphic pressure-temperature histories within the Trans-Hudson Orogen's hinterland, southwest Baffin Island, Nunavut

A.J. Smye, M.R. St-Onge, and D.J. Waters

Geological Survey of Canada

Current Research 2009-6

2009

**Geological Survey of Canada
Current Research 2009-6**



Contrasting metamorphic pressure-temperature histories within the Trans-Hudson Orogen's hinterland, southwest Baffin Island, Nunavut

A.J. Smye, M.R. St-Onge, and D.J. Waters

2009

©Her Majesty the Queen in Right of Canada 2009

ISSN 1701-4387

Catalogue No. M44-2009/6E-PDF

ISBN 978-1-100-13024-8

A copy of this publication is also available for reference in depository libraries across Canada through access to the Depository Services Program's Web site at <http://dsp-psd.pwgsc.gc.ca>

A free digital download of this publication is available from GeoPub:
http://geopub.nrcan.gc.ca/index_e.php

Toll-free (Canada and U.S.A.): 1-888-252-4301

Recommended citation

Smye, A.J., St-Onge, M.R., and Waters, D.J., 2009. Contrasting metamorphic pressure-temperature histories within the Trans-Hudson Orogen's hinterland, southwest Baffin Island, Nunavut; Geological Survey of Canada, Current Research 2009-6, 18 p.

Critical reviewer

N. Wodicka

Authors

A.J. Smye (as859@cam.ac.uk)
Department of Earth Sciences
University of Cambridge
Downing Street, Cambridge, U.K.
CB2 3EQ

D.J. Waters (dave.waters@earth.ox.ac.uk)
Department of Earth Sciences
University of Oxford
Parks Road, Oxford, U.K.
OX1 3PR

M.R. St-Onge (mstonge@nrcan.gc.ca)
Geological Survey of Canada
601 Booth Street
Ottawa, ON K1A 0E8

Correction date:

**All requests for permission to reproduce this work, in whole or in part, for purposes of commercial use, resale, or redistribution shall be addressed to: Earth Sciences Sector Copyright Information Officer, Room 644B, 615 Booth Street, Ottawa, Ontario K1A 0E9.
E-mail: ESSCopyright@NRCan.gc.ca**

Contrasting metamorphic pressure-temperature histories within the Trans-Hudson Orogen's hinterland, southwest Baffin Island, Nunavut

A.J. Smye, M.R. St-Onge, and D.J. Waters

Smye, A.J., St-Onge, M.R., and Waters, D.J., 2009. Contrasting metamorphic pressure-temperature histories within the Trans-Hudson Orogen's hinterland, southwest Baffin Island, Nunavut; Geological Survey of Canada, Current Research 2009-6, 18 p.

Abstract: A field-based structural and metamorphic study of supracrustal units situated within the Meta Incognita microcontinent of the Trans-Hudson Orogen has delineated the thermotectonic evolution of an obliquely exposed Paleoproterozoic passive-margin sequence on southwest Baffin Island. East of the Foxe Peninsula, the margin is dominated by a carbonate-clastic succession: the Lake Harbour Group. S_1 orthopyroxene-bearing assemblages within metapelitic horizons yield thermobarometric estimates of about 6 kbar, 820°C for peak conditions on a decompressive P-T path. Supracrustal units exposed farther west on the Foxe Peninsula of Baffin Island comprise the quartzose Lona Bay sequence and overlying metavolcanic-metasedimentary Schooner Harbour sequence. Metamorphic modelling of an S_2 metapelitic unit belonging to the Schooner Harbour sequence yields an anticlockwise P-T pathway with peak metamorphic conditions of about 4 kbar, 620°C. Spatially progressive differences in P-T pathways within southwest Baffin Island are accounted for by variation in the relative temporal relationship between magmatic activity and the onset of accretionary orogenesis.

Résumé : Une étude structurale et métamorphique fondée sur des levés sur le terrain des unités supracrustales situées dans le microcontinent Meta Incognita de l'orogène trans-hudsonien a permis de déterminer l'évolution thermotectonique d'une séquence de marge passive du Paléoprotérozoïque s'exprimant en surface par une coupe oblique, dans le sud-ouest de l'île de Baffin. À l'est de la péninsule Foxe, la marge est dominée par une succession de roches carbonatées et clastiques, le Groupe de Lake Harbour. Les estimations thermobarométriques sur les paragenèses à orthopyroxène définissant S_1 au sein des horizons métapélitiques indiquent une pression d'environ 6 kbar et une température de 820 °C pour les conditions maximales sur un cheminement P-T de régime de décompression. Les unités supracrustales affleurant plus loin à l'ouest dans la péninsule Foxe de l'île de Baffin sont constituées de la séquence quartzeuse de Lona Bay et de la séquence sus-jacente de roches métavolcaniques et métasédimentaires de Schooner Harbour. La modélisation métamorphique de la paragenèse définissant S_2 dans une unité métapélitique faisant partie de la séquence de Schooner Harbour indique un cheminement P-T antihoraire avec des conditions métamorphiques maximales d'environ 4 kbar et 620 °C. Dans le sud-ouest de l'île de Baffin, les différences progressives spatiales dans les cheminements P-T s'expliquent par la variation de la relation temporelle relative entre l'activité magmatique et le début de l'orogénèse accréctionnaire.

INTRODUCTION

Pressure-temperature (P-T) paths act as powerful tools in constraining the tectono-metamorphic history of a terrain (e.g. Forbes et al., 2005). Combining P-T pathways with field-based observations helps elucidate a region's orogenic evolution and provides insight into the thermal and tectonic structure of an orogen. This study takes such an approach to investigate the metamorphic and structural evolution of two areas situated at different structural levels within the Paleoproterozoic Trans-Hudson Orogen's hinterland, and in doing so, addresses variations in the orogen's tectonic and thermal architecture exposed on southwest Baffin Island. This contribution presents structural, petrological, and thermobarometric results based on targeted fieldwork carried out as part of the Southwest Baffin Island Integrated Geoscience Project (SWBIG) in the summer of 2006. The SWBIG study area extends to over 30 000 km² of southwest Baffin Island, Nunavut (Fig. 1) and is part of an ongoing effort by the Geological Survey of Canada (GSC) and its territorial and university partners to address the scarcity of accurate and recent geological knowledge in parts of the Canadian North. Supporting studies based on the SWBIG field season include detailed maps and reports on bedrock lithologies (St-Onge et al., 2007b, c; Sanborn-Barrie et al., 2008) and their structural evolution (M. Sanborn-Barrie, work in progress), alongside isotopic (J. Whalen, work in progress) and geochronological investigations (Rayner et al., 2007, 2008; N. Wodicka, work in progress).

THE TRANS-HUDSON OROGEN

The Trans-Hudson Orogen (Hoffman, 1988; Lewry and Collerson, 1990) is a Paleoproterozoic (1825–1795 Ma; St-Onge et al., 2007a) continental collision belt bearing a striking resemblance in both architecture and scale to the Cenozoic Himalaya-Karakoram-Tibetan Orogen (St-Onge et al., 2006). The Trans-Hudson Orogen spans approximately 4600 km along strike, running from central North America to the continent's northeastern edge, and is more than 800 km wide in parts. The orogen juxtaposes a lower plate, comprising the Archean Superior craton, against an amalgamation of upper-plate cratons and microcontinents (St-Onge et al., 2006). The work presented in this paper focuses on an exceptionally well-exposed segment of the Trans-Hudson Orogen's upper-plate accretionary domain, which previous studies suggest comprises a microcontinent (Meta Incognita; St-Onge et al., 2000), on southwest Baffin Island (Fig. 1).

GEOLOGY OF SOUTHWEST BAFFIN ISLAND

The eastern study area is on the southern coast of Baffin Island, east of the Foxe Peninsula (eastern study area; Fig. 1) and is separated by 220 km from the western study area on the peninsula's extreme western coast (western study area; Fig. 1). The geographic spacing of these two study areas affords an insight into spatially progressive variations in

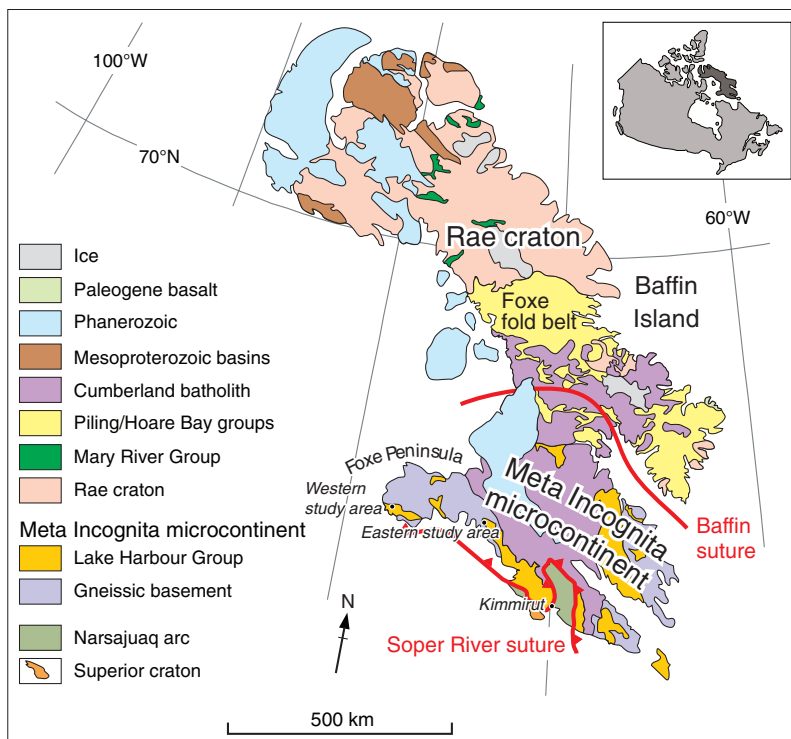


Figure 1. Regional geology of Baffin Island showing the location of the eastern and western study areas, the Meta Incognita microcontinent terrane and the upper plate, Archean Rae craton. (Modified after St-Onge et al., in press).

both the tectonic and metamorphic evolution of supracrustal units within the upper plate of Trans-Hudson Orogen (Meta Incognita microcontinent segment).

Eastern study area

The eastern study area (Fig. 2) comprises an approximately 4.5 km thick sequence of metamorphosed sedimentary rocks belonging to the Paleoproterozoic (<1.93 Ga) passive margin Lake Harbour Group (LHG; Scott et al., 2002). Field observations of structural fabrics and depositional features show that the succession faces northeast. The western part of this area is dominated by a voluminous plutonic intrusion of biotite (\pm hornblende \pm orthopyroxene) monzogranite (Fig. 3a), which hosts dioritic phases (Fig. 3b). Structurally lowest within the metasedimentary succession is a package of garnet-bearing feldspathic quartzite (Fig. 3c), overlain by 50 to 100 m of rusty silicate-facies iron formation, which is intercalated with more argillaceous horizons. Together these units form the lower Lake Harbour Group (LLHG). The overlying middle Lake Harbour Group (MLHG) comprises carbonate strata containing both dolomitic and calcitic marble interspersed with refractory layers of calc-silicate to semi-pelite (Fig. 3d). In apparent stratigraphic contact with the MLHG is the upper Lake Harbour Group (ULHG) – a succession of migmatized pelitic to psammitic clastic rocks (Fig. 3e, f), which show classic gradational bedding from coarse, siliceous bases to fine, argillaceous tops, diagnostic of turbidite deposition. Monzogranitic veins are ubiquitous throughout the area and intrude all lithologies.

Rocks within the eastern study area (Fig. 2) have undergone a polyphase deformation history as documented by multiple generations of folding, most clearly observed within carbonate units. The regionally pervasive foliation is defined by the alignment of high-temperature mineral assemblages (subsets of K-feldspar-garnet-cordierite-orthopyroxene-quartz-biotite-plagioclase) and is interpreted as being a result of transposition of a bedding fabric (S_0). This northwest-striking, moderately steeply dipping ($\sim 45^\circ$) fabric (S_1) is also present within the granitic intrusion, which dominates the western part of the study area. S_1 in rocks of the M-LLHG is folded into an asymmetrical north-northwest-trending anticline-syncline pair (F_2 folds), whose plunge is variable upon location, as determined by a further generation of cross-folding (F_3) folds. This fold interference pattern occurs as a result of crustal shortening: firstly, in a northeast-southwest direction, attributed to a D_2 event, and secondly, from a reorientation of the principle axes of stress to facilitate north-northwest-south-southeast compression within a D_3 event. Other than the S_1 fabric, observable field evidence for a D_1 event is lacking within this area. Difference in rheological behaviour between the clastic-dominated ULHG, the intrusive plutonic suite, the quartzose LLHG, and the less competent, carbonate bearing MLHG members generates a concertina-style folding pattern and suggests that deformation within the more rigid ULHG and plutonic bodies has

been accommodated via shear, both internally and along the unit boundaries. Within the northeast corner of the area, a north-northwest-striking thrust fault and associated, northeast-plunging, hanging-wall antiform dominate the structure. The thrust fault is inferred on the basis of the stratigraphic repetition of the M-LLHG units and its orientation is suggestive of a D_2 origin.

Western study area

The western study area (Fig. 4) consists of a diverse range of plutonically punctuated metasedimentary and metavolcanic supracrustal lithologies within an east-west-trending sequence of thrust imbricate panels. Geochemical studies focusing on the mafic- to intermediate volcanic rocks of the Schooner Harbour sequence (J. Whalen, work in progress) suggest a rifted margin environment of accumulation.

The structurally lowest domain exposed consists of a leucocratic and prominently bedded sillimanite-K feldspar-bearing quartzite (Lona Bay sequence; Fig. 5a). An east-west-striking thrust fault separates the quartzite from a hanging-wall sequence of hornblende-clinopyroxene amphibolite interlayered with andalusite- and garnet-bearing mica schist (the Schooner Harbour sequence; Fig. 5b). Northward, a further east-west-striking thrust fault juxtaposes a sillimanite-aggregate-bearing arkosic lithology (Fig. 5c), with the underlying amphibolite and mica schist. In turn, the arkosic unit is in close association with muscovite-biotite-garnet pelite (Fig. 5d), found farther to the north. The area's central portion is occupied by a voluminous body of biotite \pm hornblende monzogranite (Fig. 5e), which hosts abundant metasedimentary rafts and schlieren (cm to m scale). In light of new geochronological work reported in Rayner et al. (2007, 2008) and Wodicka et al. (2008a), it is unlikely that this plutonic body is a phase of the regionally ubiquitous 1865–1848 Ma Cumberland batholith (Jackson et al., 1990; Wodicka and Scott, 1997; Scott and Wodicka, 1998; St-Onge et al., 2007c), but rather, that it was emplaced during a separate phase of magmatism within the period, 1.84 to 1.83 Ga. Consequently we interpret the granite as belonging to the younger suite of the Narsajuaq arc, which is described as having been emplaced in an Andean-type continental arc setting between approximately 1842 and 1820 Ma (Dunphy and Ludden, 1998; Thériault et al., 2001; St-Onge et al., 2006). North of the intrusion, several laterally continuous bands of marble and calc-silicate (~ 200 m thick) are interlayered with biotite-cordierite-sillimanite-garnet-bearing pelitic gneiss and biotite-muscovite-sillimanite schist in the structurally highest unit exposed (Fig. 5f).

All rock units within the area are foliated, with the state of strain varying from weak in the plutonic rocks, to moderate in more pelitic horizons. The pervasive foliation is inferred to be an intensification of a primary bedding fabric in metasedimentary rocks ($S_0 + S_1$). This predominantly northward-dipping (50 – 80°) foliation is also seen within the monzogranite intrusion, where it is defined by the

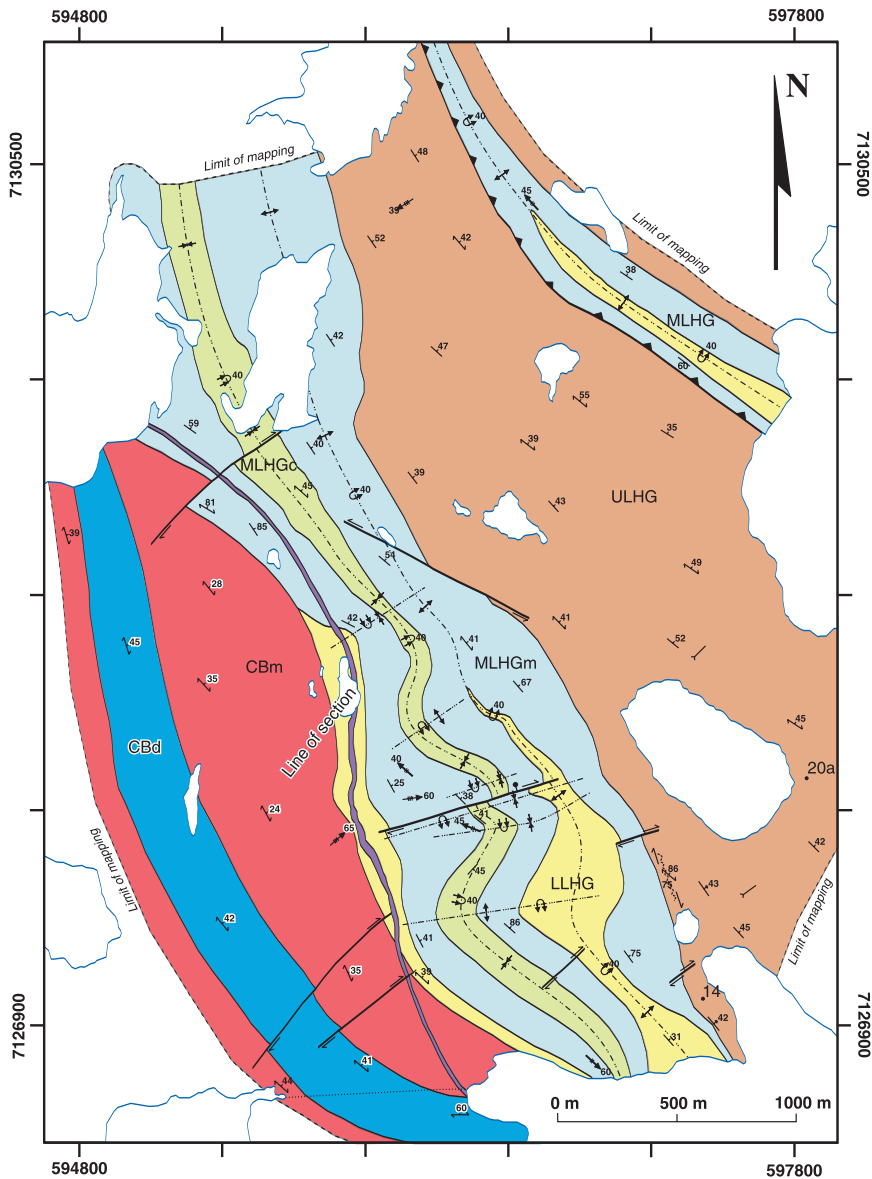


Figure 2. Geological map of the eastern study area with location of samples described in the text (see Fig. 1 for location).

LEGEND






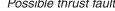








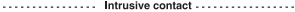
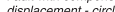
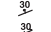
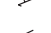
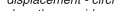

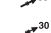



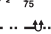


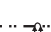
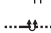
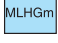
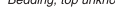






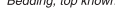





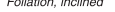




	LATE INTRUSIVE UNITS Bull quartz vein		Geological boundary		
PALEOPROTEROZOIC			Oblique-slip fault, dextral slip		
CUMBERLAND BATHOLITH (1865 - 1848 Ma)			Lineament		
	Cbm Biotite +/- orthopyroxene +/- hornblende monzogranite		Possible thrust fault		
	CBd Biotite-hornblende +/- orthopyroxene +/- clinopyroxene +/- magnetite diorite		Fault with component of normal displacement - circle indicates downthrown side		
	Intrusive contact		Bedding, top unknown, inclined		
LAKE HARBOUR GROUP (< 1934 Ma)			Bedding, top known, inclined		
	ULHG UPPER LAKE HARBOUR GROUP Psammitic, semi-pelite - turbidite sequence		Foliation, inclined		
	MLHGc MID-LAKE HARBOUR GROUP Calc-silicate, marble - pervasively intruded by biotite monzogranite		Stratigraphic younging direction, from graded bedding		
	MLHGm MID-LAKE HARBOUR GROUP Marble, dolomite, marl		F_2 mesoscopic fold axis (plunging)		
	LLHG LOWER LAKE HARBOUR GROUP Feldspathic arenite, silicate-facies iron formation, pelite		F_3 mesoscopic fold axis (plunging)		
			Shear zone, C-S planes defined		
			D_2 antiform, approximate (upright, overturned)		
			D_2 synform, approximate (upright, overturned)		
			D_3 antiform, approximate (upright, overturned)		
			D_3 synform, approximate (upright, overturned)		
			Key sample location		



Figure 3. Eastern study area lithologies. **a)** biotite-hornblende-orthopyroxene-bearing monzogranite associated with the Cumberland batholith and exposed in the western portion of the Eastern study area; **b)** phenocrystic hornblende-orthopyroxene-clinopyroxene-bearing diorite; **c)** garnet-bearing feldspathic quartzite located at the base of the Lake Harbour Group. Note the compositional layering fabric, which is interpreted as transposed primary bedding; **d)** interbedded calc-silicate and dolomite marble of the middle Lake Harbour Group. Note the refractory rinds of K-feldspar-rich calc-silicate (inset) and their concertina-style folding; **e)** banded migmatite gneiss of the upper Lake Harbour Group turbidite sequence. Leucocratic domains are dominated by quartzofeldspathic melt, whereas rusty horizons are micaceous in composition; **f)** garnetiferous migmatite gneiss from the upper Lake Harbour Group. Note the close spatial association between garnet blasts and melt selvages. Scale: the hammer used in photographs c, d, e, and f is 35 cm in

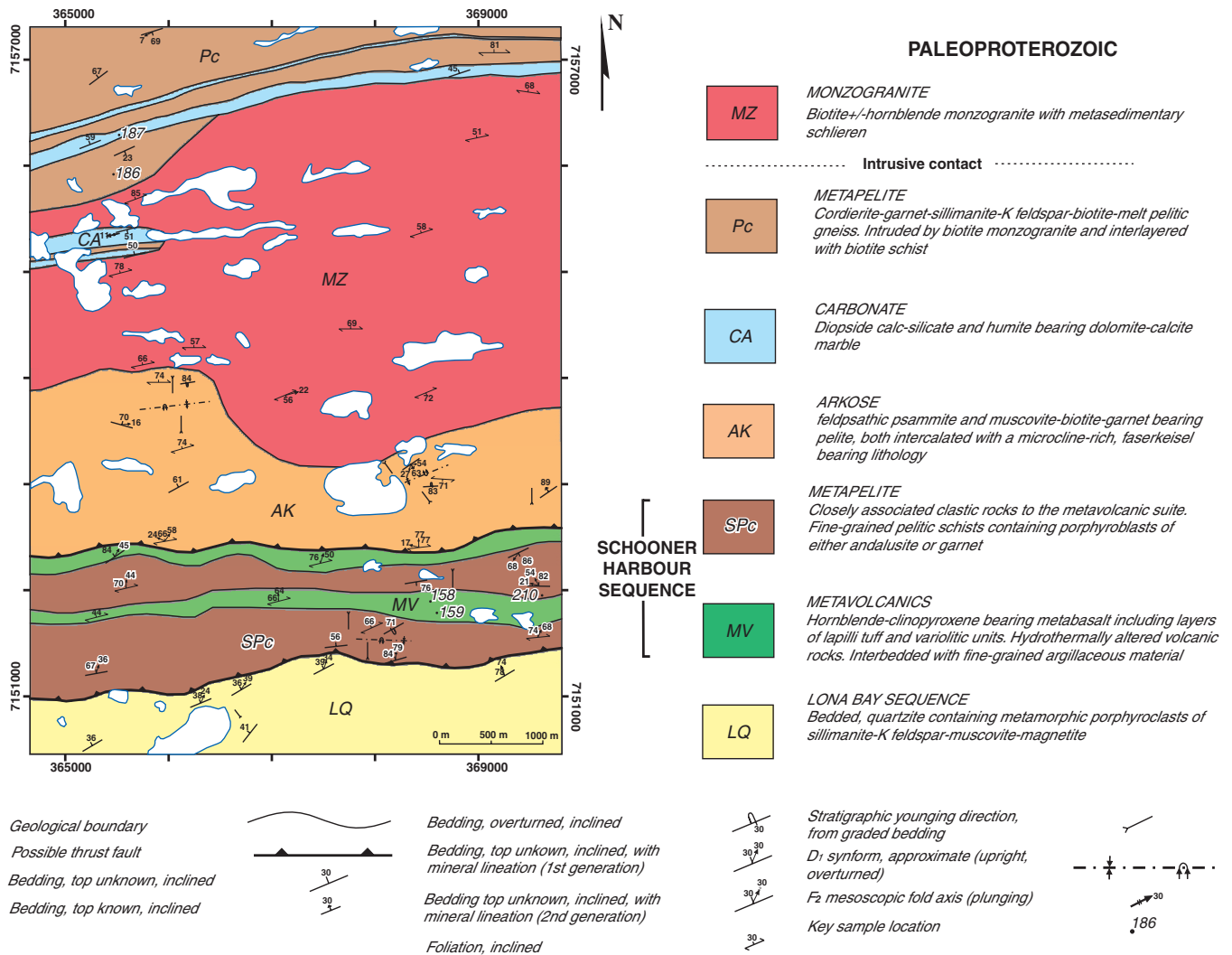


Figure 4. Geological map of the western study area with location of samples described in the text (see Fig. 1 for location).

alignment of biotite domains and K-feldspar porphyroblasts. This offers a first-order constraint on the timing of the intrusion relative to the region's deformation history. In addition, nowhere is the mapped intrusion observed to cross-cut the tectonic boundary between the Schooner Harbour sequence and the described arkosic map unit. Bedding/cleavage relationships within upright stratigraphy yield useful information regarding the presence of folds in apparently homoclinal portions of strata. Lineation measurements in conjunction with mapped fold axes suggest that moderately to steeply dipping thrust planes and hanging-wall folding define an imbricate stack structure, formed via north-south compression. Regional considerations and monazite dating of mineral assemblages and fabrics (Rayner et al., 2008; see below) suggest that this orientation of compression at about 1.82 Ga is likely to be related to a regional D₂ event, interpreted by St-Onge et al. (2007a) as related to the principal collisional event of Trans-Hudson Orogen.

Tectonostratigraphy of southwest Baffin Island

The Lake Harbour Group is one of three supracrustal sequences observed on southwest Baffin Island (St-Onge et al., 2007b) and it can be traced along strike from the eastern study region to its type locality in the vicinity of the Hamlet of Kimmirut, located farther southeast along the southern coast of Baffin Island (Fig. 1; Scott et al., 1997). The two other supracrustal sequences recognized on the basis of SWBIG fieldwork are the Lona Bay sequence and the overlying Schooner Harbour sequence, both of which are exposed within the southwestern portion of the Foxe Peninsula (Fig. 4; St-Onge et al., 2007b, c). As a result of an intervening culmination of plutonic rocks, the relationship between the principal expanse of Lake Harbour Group units in the east and the Lona Bay and Schooner Harbour sequences in the west, is unclear. However, rocks from the Lona Bay sequence show similarities to the foreland-basin

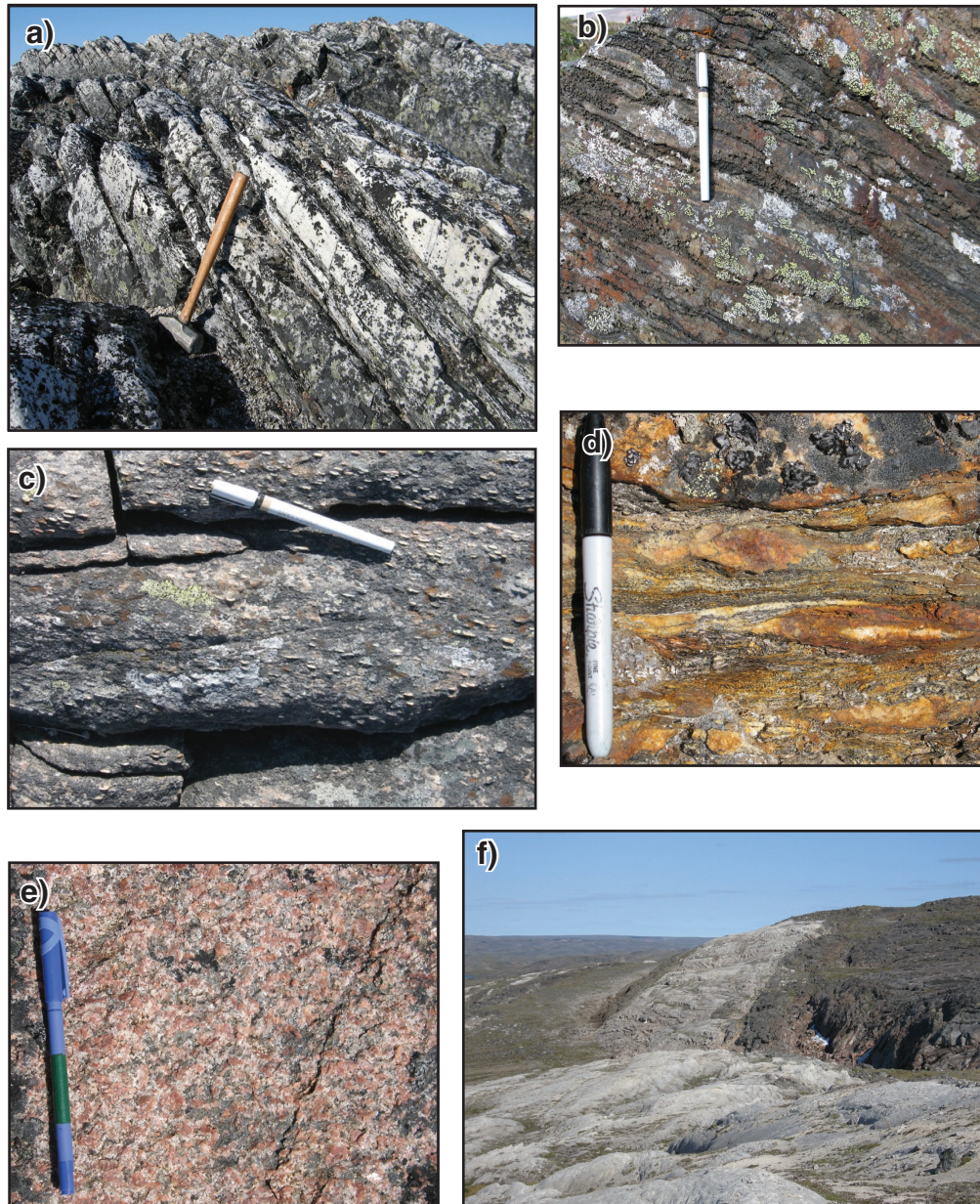


Figure 5. Western study area lithologies. **a)** Lona Bay quartzite, which contains abundant sillimanite-muscovite-K-feldspar-magnetite aggregates (faserkiesel) and displays a well defined bedding fabric; **b)** volcanic rocks of basaltic composition within the Schooner Harbour sequence. Lapilli tuff and variolitic units are intercalated with pelitic horizons and suggest a flow-related mode of origin for the volcanic rocks; **c)** arkosic psammite is interbedded with a sillimanite-aggregate-bearing, microcline-rich unit; **d)** biotite-sillimanite-garnet schist belonging to pelitic horizons observed in the northernmost portion of the field area. Note the presence of elongate melt pods and their relation to the micaceous fabric; **e)** porphyroblastic biotite-hornblende monzogranite, interpreted as part of the younger suite of Narsajuaq arc; **f)** band of diopside-bearing marble striking east-west. Note the sharp stratigraphic contact between the marble and adjacent pelitic units.

Blandford Bay assemblage (Sanborn-Barrie et al., 2008), which overlies the Lake Harbour Group farther to the east of the SWBIG project area (Scott et al., 1997), and on this basis the Lona Bay sequence can be tentatively inferred to be younger than the Lake Harbour Group (St-Onge et al., 2007b, c). An alternative interpretation, based on recently acquired detrital zircon data, is that the Lona Bay and Schooner Harbour sequences predate deposition of the Lake Harbour Group (Wodicka et al., 2008b). Further analytical work is planned to address this issue (Wodicka, work in progress). Plutonic units dominate the bedrock geology of southwest Baffin Island and commonly intrude supracrustal members. Orthopyroxene±clinopyroxene±hornblende±biotite monzogranites along with biotite-magnetite monzogranites constitute the majority of plutonic rock exposure, with the granites belonging to at least two distinct suites; the 1865 to 1848 Ma Cumberland batholith, and the younger suite of Narsajuaq arc, bracketed between 1842 and 1820 Ma (Jackson et al., 1990; Wodicka and Scott, 1997; Dunphy and Ludden, 1998; Scott and Wodicka, 1998; Thériault et al., 2001; St-Onge et al., 2006; St-Onge et al., 2007c).

ANALYTICAL METHODS

Samples suitable for petrographic analysis from both study areas were selected for thin-section cutting following splitting of the larger (>12 kg) samples using a hydraulic press. Preliminary optical petrography was undertaken using a binocular microscope. Sections appropriate for thermobarometric work were selected for mineral chemistry analysis at the University of Oxford using a JEOL JSM-840A Scanning Electron Microscope fitted with an energy dispersive spectrometer. Conditions for analysis were 20kV accelerating voltage, 6nA beam current, a standard counting time of 120 seconds and a constant beam diameter of 2 µm (for spot analyses). A pure cobalt standard was employed for quantitative calibrations. Compositional zoning within single mineral grains was studied using both area-raster and linescan techniques. All ferromagnesian minerals present were analyzed using a core-rim transect methodology to check for chemical heterogeneity. Each analysis location within the relevant thin section was chosen for its degree of textural equilibrium and lack of alteration effects. Analyzed minerals were also selected to be separated by other mineral grain constituents so as to avoid local diffusional re-equilibration between different mineral grains. Averaging spot analyses for compositional domains within individual mineral grains generated a statistically robust chemical data set suitable for thermobarometric work.

Estimates of pressure and temperature were calculated using the activity-composition program – AX, (Holland and Powell, 1995) and THERMOCALC 3.25 software (Powell and Holland, 1988). Garnet-biotite, cation exchange thermometry (Holdaway, 2000) enabled verification of temperature

estimates. THERMOCALC was also used in phase diagram mode to construct a P-T pseudosection for sample AS06-210 from the western study area.

METAMORPHIC ASSEMBLAGES AND FABRICS

Eastern study area

In the eastern study area, metapelitic rocks from the ULHG are characterized by subsets of the granulite facies mineral assemblage: orthopyroxene-garnet-cordierite-K feldspar-plagioclase-biotite-quartz-melt. The distribution of the subset assemblages is strongly domainal, as defined by cm-scale compositional banding in which seams of quartzofeldspathic leucosome alternate with biotite-rich domains of paleosome. Poikiloblastic garnet (5–10 mm diameter) is chaotically located proximal to the boundaries of melt selvages. Rare, elongate orthopyroxene grains (3–10 mm length) mantle neosome patches and are associated with garnet and cordierite grains. Cordierite is present in both porphyroblast (3–5 mm diameter) and matrix constituent (<1 mm diameter) form. Larger porphyroblasts are generally heavily pinnitized, whereas the finer granoblastic cordierite displays a fresh appearance. Large (10 mm diameter) porphyroblasts of K-feldspar (microcline-perthite) occur within coarse-grained neosome portions of the migmatite. The matrix domain is dominated by a fine-grained (1 mm diameter) aggregate of granoblastic quartz and plagioclase with minor cordierite. Aligned biotite flakes (1–2 mm length) are abundant throughout the matrix and define the pervasive fabric, $S_0 + S_1$. Coarser (3–5 mm length) flakes of secondary biotite with a characteristic ‘spongy’ appearance, form clusters around the edges of melt selvages, indicative of a period of back-reaction with the melt-phase at high temperatures. Easily recognizable sillimanite is absent, with the exception of rare and small populations of remnant, specular blades within zones of alteration. Graphite occurs throughout as an abundant accessory phase and is present as large, elongate flakes (2–10 mm length), aligned parallel to the gneissosity. More aluminous horizons are characterized by the occurrence of small (2–3 mm diameter) euhedral grains of spinel in close association with similar sized grains of dusty cordierite. Monazite and zircon are present as fine inclusions (0.6–0.8 mm length), both within neosome and paleosome domains; apatite is much less common.

The MLHG unit displays both a diverse and disparate range of carbonate-calc-silicate lithologies. Metacarbonate is characterized by subsets of the mineral assemblage: calcite-dolomite-forsterite-diopside-phlogopite-quartz. Calcite is the dominant matrix constituent (>50%) and forms a homogeneous granoblastic matrix domain with varying quantities of dolomite (5–50%). Matrix grain size varies from fine (0.5 mm diameter) to medium (5–6 mm diameter). However, the fused and idioblastic nature of both carbonate minerals

is consistent throughout the marble suite and is suggestive of dynamic recrystallization. Euhedral flakes of coarse (1–5 mm length) phlogopite occur as porphyroblasts and exhibit bent basal cleavages. The presence of both diopside and forsterite together indicates that the dolomitic marble has experienced high-grade metamorphic conditions (Yardley, 1989). Forsterite is more common than diopside and occurs as medium-grained (2–4 mm diameter) porphyroblasts within the fine-grained matrix. Extensive serpentinization of olivine is indicative of interaction with hydrothermal fluids post metamorphic growth. Diopside occurs as heavily reworked, refractory porphyroblasts (2–3 mm length).

Calc-silicate units show subsets of the high-temperature mineral assemblage calcite-dolomite-wollastonite-diopside-K-feldspar-quartz-scapolite-sphene. These assemblages are distributed in a curious domainal nature, which comprises a very fine-grained, subrounded calcite matrix in which two different morphologies of composite lithic clasts occur. Clasts of carbonate affinity contain parts of the high-temperature assemblage calcite-dolomite-wollastonite-scapolite-diopside. Wollastonite is the main clast constituent and occurs as large blasts, closely associated with scapolite grains. Diopside is less abundant, but displays a similarly heavily reworked appearance, as observed in the marble units. The siliceous component is represented by brecciated clasts of K-feldspar and quartz. Large blasts (6–3 mm diameter) of K-feldspar display distinctive exsolution textures consisting of albite lamellae within a perthitic host grain. The calcite-dominated matrix has undergone extreme dynamic recrystallization and appears to flow around refractory lithic clasts to form a chaotic mylonitic mélange of both siliceous and carbonate rock types.

Western study area

In the western study area, horizons of pelite-semipelite interbedded with both metavolcanic rocks of the Schooner Harbour sequence and carbonate-bearing units to the north (Fig. 4) contain metamorphic assemblages that can be directly compared with those of the eastern study area.

Pelite is characterized by subsets of the middle-amphibolite facies mineral assemblage: garnet-andalusite-cordierite-biotite-muscovite-sillimanite-plagioclase-quartz. Garnet forms abundant idioblastic poikiloblasts with fine-grained internal quartz-plagioclase±biotite-monazite inclusion trails that are oriented obliquely to the external foliation. An inclusion-free rim to some garnet poikiloblasts is closely associated with weakly sigmoidal trails. This relationship suggests that synkinematic garnet growth occurred and that blast reorientation facilitated a generation of inclusion-free growth. Large (25–40 mm length) andalusite poikiloblasts contain similarly oriented quartzofeldspathic inclusion trails. However, andalusite and garnet are not seen together within the same rock. Both andalusite and garnet poikiloblasts disrupt the pervasive micaceous foliation, which is significantly flattened around refractory phases via a crenulation cleavage.

Common in the pelitic domains is a heavily micaceous matrix. Biotite is generally more abundant than muscovite and forms elongate, euhedral (0.3–1.5 mm length) flakes or blades, depending on local strain intensity. Two morphologies of muscovite are present: matrix muscovite occurs in a similar euhedral form as matrix biotite, whereas secondary, retrograde, muscovite is present in clusters, as coarse flakes (2–5 mm length). Interstitial quartz, showing minor undulose extinction, and plagioclase constitute the remainder of the schistose matrix domain, which houses rare and heavily altered lozenges of porphyroblastic cordierite (1–2 mm diameter). Fibrous, fine-grained (0.05–0.2 mm length), sillimanite needles occur as uncommon patches within the matrix. Sillimanite is also present as a minor, but interesting, overgrowth on the corners of andalusite poikiloblasts, indicating a prograde, low-pressure ascent in temperature. Minor, specular tourmaline (0.2–0.3 mm length), along with shards of graphite (0.1–1 mm diameter) occur within the matrix. Further accessory phases include locally abundant inclusions of zircon and monazite along with minor apatite.

Well developed porphyroblast-matrix relations indicate a polyphase deformation history compatible with field observations (Sanborn-Barrie et al., 2008). Internal inclusion trail fabrics, defined by aligned quartz grains (0.2–0.5 mm diameter), within garnet and andalusite porphyroblasts represent the earliest stage of fabric development present and can be attributed to $S_0 + S_1$, a compositional layering fabric. The pervasive, muscovite-defined matrix fabric clearly visible in both garnet and andalusite schists represents $S_0 + S_1 + S_2$, which, in turn, is flattened around refractory blasts in an open crenulation fabric - $S_0 + S_1 + S_2 + S_3$. The weakly S-shaped nature of quartz inclusion trails within poikiloblasts suggests that garnet and andalusite growth initiated post $S_0 + S_1$ and continued in a synkinematic fashion prior to the onset of S_3 development (i.e. the poikiloblasts are syn- D_2 in age).

Metacarbonate and calc-silicate units in the western study area are characterized by subsets of the mineral assemblage: dolomite-calcite-K-feldspar-tremolite-diopside-phlogopite-humite-scapolite-quartz-clinozoisite. Within the marble units, dolomite is generally less abundant than calcite (~40% dol: 60% cal). Both carbonate minerals form a fine-grained (0.8–1 mm diameter), granoblastic matrix domain that is devoid of any fabric trace and evidence of significant recrystallization. Mineralogically and texturally homogeneous marble bands alternate with horizons of calc-silicate. Boundaries between these lithologies commonly display reaction zones with abundant tremolite blades (2–10 mm length) and scapolite growth. Calc-silicate units are dominated by a fine-grained (<1 mm diameter) calcite-dolomite matrix, but unlike the marble, they contain envelopes of quartz (2–5 mm width) and blasts of microcline (1–2 mm diameter). Fine (<0.5 mm wide), exsolved growths of dolomite are present within matrix host grains of calcite, commonly giving the carbonate portions a ‘spotty’ appearance. Diopside is a common phase and forms porphyroblasts (5–6 mm) with a

fresh appearance. Twinned chondrodite forms large (3 mm diameter), subhedral grains within the calc-silicate matrix, which only rarely contains flakes of phlogopite, along with minor quantities of biotite. Together, these micas define a very weak foliation - $S_0 + S_1$. Clinzoisite is present as an accessory phase and is found within matrix interstices.

MINERAL CHEMISTRY

Metapelitic samples from both study areas were selected for chemical analyses in order to facilitate the comparison and tectonic analysis of the resulting thermobarometric results.

Eastern study area

In the eastern study area (Table 1), garnet is an almandine-rich, almandine-pyrope solid solution with only minor grossular and spessartine. Garnet compositions vary from X_{alm} [Fe/(Fe + Mg + Mn + Ca)] = 0.592 (AS06-20a) to X_{alm} 0.679 (AS06-14). Values of X_{pyp} [Mg/(Fe + Mg + Mn)] range from 0.294 (AS06-14) to 0.378 (AS06-20a). A weak systematic variation in spessartine content is observed within core-rim traverses, with the garnet core being approximately 0.0015 (X_{sps}) more depleted than rim compositions. Similarly, the cores of neosome garnet poikiloblasts are approximately 0.04 (X_{pyp}) richer in pyrope than rim portions. Such weak chemical gradients are likely the result of a period of partial re-equilibration at temperatures high enough to facilitate volume diffusion (Anderson and Olimpio, 1977). This is corroborated by garnet core regions being slightly depleted in Mn relative to rim portions.

Core aluminum compositions are about 20–25% higher than rim values within orthopyroxene porphyroblasts (0.173 - core, AS06-20a; 0.142 - rim, AS06-20a). As a result of aluminum's refractory nature and its ability to withstand the effects of volume diffusion, these chemical gradients are taken to represent a prograde growth zonation pattern (Pattison et al., 2003).

Independent of textural setting, cordierite is compositionally homogeneous (samples AS06-14 and AS06-20a).

Biotite inclusions within garnet poikiloblasts are more magnesian (X_{Mg} [Mg/(Mg + Fe)] = 0.766–0.763) than matrix biotite (X_{Mg} = 0.647–0.690). Plagioclase is albite rich throughout, with values of X_{ab} [Na/(Na + Ca)] ranging from 0.794 to 0.686. Most variation reflects a slight core-to-rim decrease in X_{ab} . Alkali feldspar is abundant throughout the granulite facies metapelitic rocks and is an orthoclase-rich solid solution, with values of X_K [K/(K + Na)] ranging from 0.973 to 0.737.

Western study area

In the western study area (Table 2), garnet is an almandine-rich solid solution with values of X_{alm} showing considerable variation between individual samples. In sample AS06-210, X_{alm} = 0.823–0.838 and X_{pyp} , X_{grs} , and X_{sps} vary between 0.039–0.053, 0.043–0.056, and 0.068–0.079, respectively. For sample AS06-159, X_{alm} = 0.689–0.757 and X_{pyp} , X_{grs} , and X_{sps} vary between 0.037–0.056, 0.045–0.064, and 0.146–0.212, respectively. Garnet shows partly re-equilibrated prograde growth zoning patterns in which core regions are mildly depleted in iron relative to rim portions (Spear, 1993). A frozen diffusion profile is present within porphyroblast rims where values of manganese and calcium increase in symphony with decreasing iron and magnesian values as proximity to matrix material increases.

Biotite is compositionally homogeneous in both matrix and inclusion form. Within the more iron-rich pelitic rocks, biotite X_{Mg} values are as low as 0.240 (AS06-210), whereas in more magnesian pelitic rocks, X_{Mg} values average 0.460.

Muscovite is commonly observed and has values of X_{Fe} ranging from 0.429 to 0.766, depending on individual sample. Iron is generally in excess of magnesium. Irrespective of sample, muscovite grains contain between 6.09 and 6.17 Si cations per formula unit (22 oxygen). Alongside the substitution of Fe/Mg-Si in the place of Al, Na also substitutes for K. Values of X_K commonly range between 0.92 and 0.96 indicative of muscovite grains with between 8–4 mol % paragonite.

Cordierite grains are heavily retrogressed and difficult to analyze. A composition for cordierite in equilibrium with matrix biotite was obtained for sample AS06-158 via a Fe-Mg cation reconstruction calculation, using K_D as 0.52 (cf. Bushveld Aureole, S. Africa); X_{Mg} = 0.624.

Plagioclase is essentially unzoned and compositionally independent of textural setting with X_{ab} varying between different samples from 0.602 to 0.775.

THERMOBAROMETRY

In the eastern study area (Table 3), probe sections for two representative metapelitic gneiss samples were chosen for quantitative thermobarometry, samples AS06-14 and AS06-20a (Fig. 2).

Sample AS06-14 is a banded migmatite gneiss containing an S_1 granulite facies mineral assemblage of: orthopyroxene-cordierite-garnet-biotite-K-feldspar-quartz-plagioclase-melt. Chemical analyses of biotite, cordierite, garnet, orthopyroxene, K-feldspar and plagioclase generate six independent equilibria, which yield average P-T

Table 1. Selected representative SEM mineral analyses from eastern study area granulites.

	AS06-14										AS06-20a									
	Grt _{fin}	Grt _{core}	Crd	Kfs	Pl	Bt _{matrix}	Bt _{inclusion}	Opx _{fin}	Opx _{core}		Grt _{fin}	Grt _{core}	Crd	Kfs	Pl	Bt	Opx _{fin}	Opx _{core}		
SiO ₂	39.23	39.13	49.47	66.49	64.95	38.57	38.74	51.26	50.40		39.06	39.27	48.97	66.31	62.14	38.23	51.63	51.48		
TiO ₂	0.03	0.02	0.01	0.12	0.04	6.46	7.09	0.12	0.18		0.04	0.05	0.01	0.13	0.00	6.35	0.16	0.16		
Al ₂ O ₃	22.02	22.10	34.07	19.40	23.71	14.59	15.14	3.87	4.75		22.05	22.34	33.61	19.33	24.95	14.62	3.23	4.01		
Fe ₂ O ₃	0.81	1.34	0.93	0.05	0.05	0.00	0.00	0.52	0.00		1.22	1.42	0.90	0.02	0.09	0.00	0.00	0.00		
FeO	29.66	29.21	4.77	0.00	0.00	13.06	9.41	25.69	25.62		29.35	28.03	4.60	0.00	0.00	11.77	25.31	25.33		
MnO	0.26	0.28	0.01	0.00	0.00	0.04	0.03	0.08	0.06		0.38	0.31	0.01	0.16	0.00	0.01	0.09	0.11		
MgO	9.04	9.21	10.47	0.00	0.00	15.08	17.08	19.89	19.42		8.83	9.80	10.48	0.04	0.00	15.77	20.21	20.24		
CaO	0.70	0.70	0.01	0.31	4.33	0.06	0.03	0.07	0.04		0.99	0.93	0.02	0.13	5.98	0.06	0.08	0.09		
Na ₂ O	0.00	0.00	0.00	2.72	9.13	0.00	0.07	0.00	0.00		0.00	0.00	0.00	0.64	7.54	0.03	0.00	0.00		
K ₂ O	0.00	0.00	0.00	13.72	0.12	10.74	10.47	0.03	0.00		0.00	0.00	0.00	16.99	0.26	10.74	0.01	0.00		
Total	101.75	101.99	99.74	102.81	102.33	98.60	98.06	101.53	100.47		101.74	101.95	98.42	103.74	100.88	97.58	100.67	101.40		
Calculated ions num. ox.	12	12	18	8	8	11	11	6	6		12	12	18	8	8	11	6	6		
Si	2.99	2.97	4.95	2.97	2.80	2.77	2.75	1.91	1.89		2.97	2.96	4.95	2.97	2.73	2.76	1.93	1.91		
Ti	0.00	0.00	0.00	0.00	0.00	0.35	0.34	0.00	0.01		0.00	0.00	0.00	0.00	0.00	0.35	0.00	0.00		
Al	1.98	1.98	4.02	1.02	1.21	1.24	1.27	0.17	0.21		1.98	1.99	4.01	1.02	1.29	1.25	0.14	0.18		
Fe ³⁺	0.05	0.08	0.07	0.00	0.00	0.00	0.00	0.01	0.00		0.07	0.08	0.07	0.00	0.00	0.00	0.00	0.00		
Fe ²⁺	1.89	1.86	0.40	0.00	0.00	0.79	0.56	0.80	0.80		1.87	1.77	0.39	0.00	0.00	0.71	0.79	0.79		
Mn	0.02	0.02	0.00	0.00	0.00	0.00	0.00	0.00	0.00		0.02	0.02	0.00	0.01	0.00	0.00	0.00	0.00		
Mg	1.03	1.04	1.56	0.00	0.00	1.62	1.81	1.10	1.09		1.00	1.10	1.58	0.00	0.00	1.70	1.12	1.12		
Ca	0.06	0.06	0.00	0.01	0.20	0.00	0.00	0.00	0.00		0.08	0.08	0.00	0.01	0.28	0.00	0.00	0.00		
Na	0.00	0.00	0.00	0.24	0.76	0.00	0.01	0.00	0.00		0.00	0.00	0.00	0.06	0.64	0.00	0.00	0.00		
K	0.00	0.00	0.00	0.78	0.01	0.99	0.95	0.00	0.00		0.00	0.00	0.00	0.97	0.01	0.99	0.00	0.00		
Total	8.00	8.00	11.00	5.02	4.98	7.75	7.69	4.00	4.00		8.00	8.00	11.00	5.03	4.95	7.76	3.99	4.00		
X _{alm}	0.64	0.62	X _k	0.77	0.01						X _{alm}	0.63	X _k	0.95	0.02					
X _{pyr}	0.34	0.35	X _{abb}	0.94	0.79						X _{pyr}	0.34	X _{abb}	0.90	0.70					
X _{spss}	0.01	0.01									X _{spss}	0.01								
X _{grs}	0.02	0.02									X _{grs}	0.03								
X _{fs}	0.65	0.64	0.20			0.33	0.24	0.42	0.43		0.65	0.62	0.20	0.00	0.30	0.41	0.41	0.41		

Fe³⁺ is derived from charge balance calculation

Table 2. Representative SEM mineral analyses from garnet-mica schists of the western study area.

	AS06-159					AS06-210				
	Grt _{rim}	Grt _{core}	Bt	Pl		Grt _{rim}	Grt _{core}	Bt	Mu	Pl
SiO ₂	37.57	37.20	34.01	59.40		37.21	37.08	34.28	46.19	60.04
TiO ₂	0.01	0.03	1.07	0.00		0.02	0.00	2.49	0.39	0.02
Al ₂ O ₃	21.02	20.75	19.37	25.28		21.02	20.96	19.98	36.73	26.72
Cr ² O ³	0.00	0.00	0.00	0.00		0.00	0.00	0.00	0.00	0.00
Fe ² O ³	1.81	1.63	0.00	1.69		0.66	0.87	0.00	0.00	0.19
FeO	32.03	30.12	25.81	0.00		37.11	36.28	26.10	1.45	0.00
MnO	7.40	9.60	0.20	0.04		3.04	3.51	0.06	0.01	0.00
MgO	1.35	0.96	6.01	1.20		1.00	1.21	4.63	0.36	0.00
CaO	2.34	2.18	0.10	5.18		1.97	1.76	0.04	0.05	7.91
Na ₂ O	0.00	0.00	0.02	6.08		0.00	0.00	0.10	0.29	6.88
K ₂ O	0.03	0.04	10.22	2.63		0.00	0.02	10.04	10.76	0.10
Total	103.56	102.51	96.81	101.50		102.03	101.69	97.72	96.23	101.86
Calculated ions num ox	12.00	12.00	11.00	8.00		12.00	12.00	11.00	11.00	8.00
Si	2.97	2.97	2.65	2.63		2.98	2.98	2.64	3.04	2.63
Ti	0.01	0.00	0.06	0.00		0.00	0.00	0.14	0.02	0.00
Al	21.01	1.96	1.78	1.32		1.99	1.99	1.81	2.85	1.38
Cr	0.00	0.00	0.00	0.00		0.00	0.00	0.00	0.00	0.00
Fe ³⁺	0.11	0.10	0.00	0.06		0.04	0.05	0.00	0.00	0.01
Fe ²⁺	2.16	2.01	1.68	0.00		2.49	2.44	1.68	0.08	0.00
Mn	0.50	0.65	0.01	0.00		0.21	0.24	0.00	0.00	0.00
Mg	0.16	0.16	0.70	0.08		0.12	0.15	0.53	0.04	0.00
Ca	0.20	0.19	0.01	0.25		0.17	0.15	0.00	0.00	0.37
Na	0.00	0.00	0.00	0.52		0.00	0.00	0.01	0.04	0.58
K	0.00	0.00	1.02	0.15		0.00	0.00	0.99	0.91	0.01
Total	27.12	8.04	7.91	5.01		8.00	8.00	7.81	6.98	4.97
X _{alm}	0.72	0.67	X _K	0.22	X _{alm}	0.83	0.82	X _K	0.96	0.01
X _{pyr}	0.05	0.05	X _{ab}	0.68	X _{pyr}	0.040	0.050	X _{ab}	0.93	0.61
X _{sps}	0.17	0.22			X _{sps}	0.069	0.081			
X _{grs}	0.07	0.06			X _{grs}	0.057	0.050			
X _{Fe}	0.93	0.93	0.71	0.00		0.95	0.94	0.76	0.69	

Fe³⁺ is derived from charge balance calculation

Table 3. Pressure-Temperature estimates

Sample	Lithology	P(kbar)	SD(kbar)	T(°C)	SD(°C)	Equilibria
<i>Eastern Area</i>						
AS06-14	opx-crd-gt-kfs-bt-qtz-pl migmatite gneiss	6.1	0.8	804	62	en+mgts=py; 2py+3q=crd+2en; 2alm+3q=fcrd+2fs
AS06-20a	opx-crd-gt-bt-kfs-qtz-pl migmatite gneiss	5.8	0.8	829	65	en+mgts=py; 2py+3q=crd+2en; 2alm+3q=fcrd+2fs; en+3an=gr+crd; fs+3an=gr+fcrd; 3py+2ann=3fs+3mgts+2phl
<i>Western Area</i>						
AS06-210	gt-bt-mu-qtz-pl schist	3.9	0.63	568	108	3east+6q=phl+py+2mu; phl+east+6q=py+2cel; 2ann+mu+6q=alm+3fcel; ann+3an=gr+alm+mu; 3east+3fcel=2phl+ann+3mu
				607*		
AS06-158	and-crd-bt-mu-pl-qtz schist	2.6	0.4	674	32	sill=and; 7cel+phl+18and=8mu+5crd; 8cel+east+18and=9mu+5crd; 2cel+2and=mu+east+5q; 7fcel+ann+18and=8mu+5fcrd; 2fcel+4and=2mu+fcrd+q
ASA06-159	gt-pl-bt-qtz schist			590*		
ASA06-186	gt-crd-sil-kfs-bt-pl-qtz migmatite gneiss	3.9	0.6	690	41	gr+q+2sill=3an; 2py+5q+4sill=3crd; 2alm+5q+4sill=3fcrd; py+east+3q=crd+phl; 6crd+5phl=9py+5san+5H ₂ O+3sill; 6fcrd+5ann=9alm+5san+5H ₂ O+3sill
				733*		
				671 ⁿ		
* T derived from gt-bt cation exchange thermometer (Holdaway, 2000).						
ⁿ T derived from grt-crd cation exchange thermometer (Perchuk and Lavrent'eva, 1983).						
All other thermobarometry done using THERMOCALC v.3.25 (Powell and Holland, 1988) - end-member abbreviations as used in Powell and Holland (1988).						

conditions of 6.1 kbar and 804°C (Fig. 6). This estimate assumes a two-part fluid composition of $a(CO_2) = 0.6$ and $a(H_2O) = 0.4$, which is supported by the presence of minor graphite and previous fluid composition studies (e.g. Seigny and Ghent, 1989; Vernon and Clarke, 2008). Nearest approximation to peak garnet composition is taken from just inside the porphyroblast's rim zone so as to be isolated from diffusion effects.

Sample AS06-20a is a compositionally banded migmatite gneiss containing an orthopyroxene-bearing S_1 mineral assemblage identical to that of sample AS06-14. Average P-T estimates are 5.8 kbar and 829°C (Fig. 6) with a fluid phase composition: $a(CO_2) = 0.6$, $a(H_2O) = 0.4$. This assumption is based on the same explanation used for sample AS06-14 above. Garnet-biotite thermometry generates spuriously low temperatures interpreted to be due to post-thermal peak cation exchange (Fitzsimons and Harley, 1994).

In the western study area (Table 3), four samples of aluminosilicate and garnet schist were analyzed to constrain P-T conditions within the middle-amphibolite facies terrain (Fig. 4).

Sample AS06-158 is a micaceous, porphyroblastic andalusite schist containing altered cordierite along with matrix biotite, muscovite, plagioclase and quartz. SEM analyses for biotite, plagioclase and muscovite were obtained. To generate sufficient equilibria a cordierite composition was reconstructed based on the assumption that it is in exchange

equilibrium with biotite, using $K_D^{Fe-Mg}_{Bt-Crd} = 0.52$ (Holdaway and

Lee, 1977). Six equilibria constrain the average P-T to be 2.6 kbar and 674°C (Fig. 6).

Sample AS06-210 is an intensely foliated, Fe-rich mica-schist studded with garnet poikiloblasts. Assuming the presence of an aluminosilicate, analyses from the S_2 biotite-muscovite-garnet-plagioclase-bearing assemblage provides five independent reactions to generate a loosely constrained average P-T of 3.6 kbar and 568°C. A better constrained average P of 3.9 kbar is calculated via eliminating the paragonite end-member to provide an estimate independent of $a(H_2O)$. Garnet-biotite thermometry, using inner-rim garnet and mean biotite compositions, gives a slightly higher temperature estimate of 607°C.

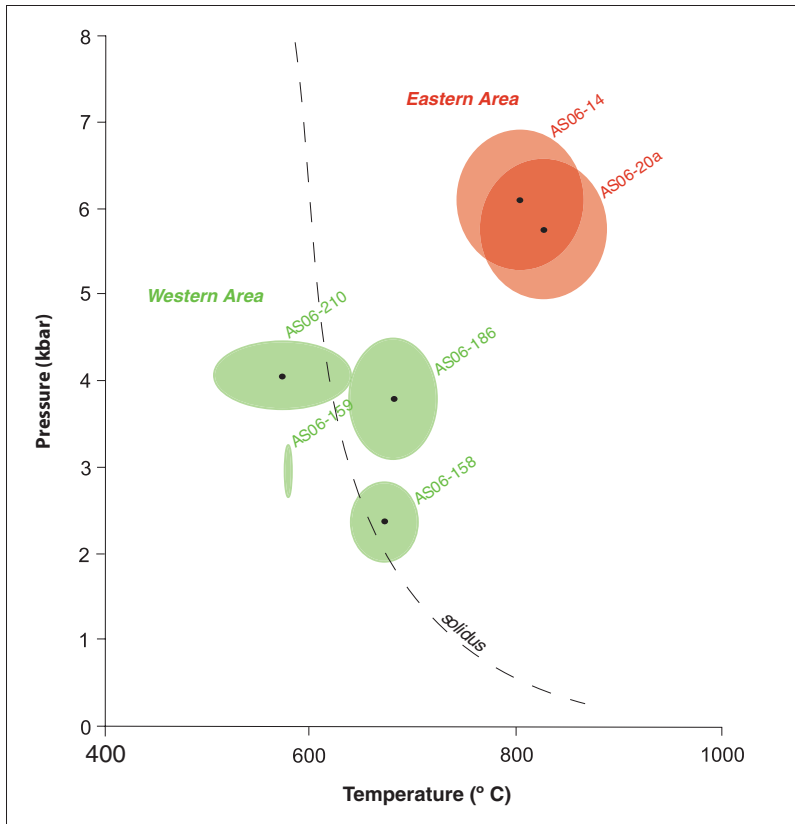


Figure 6. Summary of thermobarometric data for metapelitic rocks from both study areas (see Table 3 for absolute values). Ellipses represent error margins generated in THERMOCALC. Solidus reaction position from Hensen and Green (1971).

Sample AS06-159 is a garnet-biotite schist lacking both aluminosilicate and muscovite and therefore suitable only for thermometry. Assuming a pressure of 3 kbar, based on P calculations for adjacent samples (AS06-158 and AS06-210), a mean biotite composition together with an interior poikiloblastic garnet composition generate a temperature estimate of 590°C (Fig. 6).

Sample AS06-186 is a coarse-grained, weakly foliated, migmatite gneiss situated proximal to a plutonic body, with incipient dehydration melting textures. A garnet-sillimanite-K-feldspar-cordierite-biotite-plagioclase-quartz-bearing mineral assemblage places the rock within the high-temperature K-feldspar-sillimanite field and yields an average P-T of 3.9 kbar, 690°C. Cation exchange thermometry gives a higher temperature value of 733°C.

METAMORPHIC MODELLING

The garnetiferous metapelite samples from the western study area are suitable targets for the calculation of petrologically meaningful pseudosections (e.g. Vance and Mahar, 1998; Zuluaga et al., 2005; Caddick et al., 2007), as a result of their mineral assemblages and preserved chemical gradients within garnet porphyroblasts. In contrast, garnet within migmatite gneiss from the eastern study area is too severely affected by post-peak diffusion processes to yield significant segments of P-T path. THERMOCALC (v3.25) software (Powell and Holland, 1988) is used in conjunction with the

internally consistent thermodynamic data set of Holland and Powell (1998) to generate a pseudosection for the amphibolite facies sample AS06-210, based on the expanded model pelite system MnO-CaO-Na₂O-K₂O-FeO-MgO-Al₂O₃-SiO₂-H₂O (e.g. Tinkham et al., 2003; Fig. 7). Equilibria calculations are based on the following bulk composition for sample AS06-210, which was generated by combining modal mineral proportions with representative SEM mineral analyses: MnO - 0.27, CaO - 1.23, Na₂O - 1.00, K₂O - 4.35, FeO - 10.92, MgO - 2.85, Al₂O₃ - 13.56, SiO₂ - 65.81, with H₂O taken to be in excess.

Garnet from sample AS06-210 is an almandine-rich phase, with a core composition of 5–5.5 mol% pyrope, 4–4.2 mol% grossular and 10–10.8 mol% spessartine. A composition interpreted to be that of thermal peak conditions is taken from just inside the garnet rim, so as to minimize local retrograde diffusion effects: 5.8–6.0 mol% pyrope, 5.4–5.5 mol% grossular and 7.8–8 mol% spessartine. Mn is preferentially located in the site of first garnet growth, which infers that the core composition relates to that of earliest garnet growth in sample AS06-210.

The segment of sample AS06-210's prograde P-T evolution deduced from garnet growth modelling (Fig. 7) suggests that progressive garnet growth occurred on a compressive P-T segment within the garnet-andalusite-biotite-muscovite stability field, to attain peak conditions just within the garnet-biotite-muscovite stability field. Average P-T calculations (see previous section and Table 3) also suggest that peak conditions are within the garnet-biotite-muscovite

field, just up-P from the ‘andalusite-out’ equilibrium. The proposed P-T path, defined by pyrope and grossular isopleths (Fig. 7) is consistent with isopleths constraining garnet core composition and lies within error of near rim, peak P-T determinations. End-member interpretations of the path’s geometry are 1) a straight path between core and rim P-T values, suggesting concomitant heating and burial, and 2) a curved path, as shown on Figure 7.

P-T EVOLUTION

Pelitic rocks from the two study areas described above document petrographically and petrologically distinct metamorphic events; S_1/M_1 deformation fabrics and metamorphic assemblages in the eastern study area, versus S_2/M_2 deformation fabrics and metamorphic assemblages in the western study area. These results are consistent with the studies of St-Onge et al. (2007a) and Rayner et al. (2008) which also reported evidence of at least two metamorphic events, M_1 and M_2 , from rocks of south-southwest Baffin Island. St-Onge et al. (2007a) presented P-T estimates for peak, M_1 , granulite facies metamorphism, of between 7.5–8.4 kbar and 790–850°C, prior to a retrograde, M_2 , amphibolite facies event in Lake Harbour Group metasedimentary rocks exposed along strike of this study’s eastern area. Studies farther west on southern Baffin Island (Rayner et al., 2008) suggested that peak metamorphism, ranging from 4.8–5.6 kbar and 675–740°C, is synchronous with regional D_2 deformation following penetrative fabric development associated with D_1 .

In the eastern area, supracrustal lithologies of the Lake Harbour Group experienced a prograde P-T evolution, which culminated in granulite facies peak conditions (M_{1a} of St-Onge et al., 2007a; Fig. 8). This high-temperature event was at least partly synchronous with the development of a regionally pervasive S_1 fabric, which is interpreted as resulting from transposition of an existing compositional layering fabric, S_0 , during a D_1 event. S_1 assemblages reflect peak P-T conditions of between 5.8–6.1 kbar and 804–829°C (Fig. 6), slightly lower-P than peak conditions reported from Lake Harbour Group metapelites that outcrop along strike farther to the east on south Baffin Island. Rocks within the eastern area experienced a clockwise P-T pathway (Fig. 8), which is inferred by the close association of S_1 orthopyroxene and cordierite, thought to form through a decrease in pressure at peak temperatures (Hensen and Green, 1971, 1973). High temperatures (>550°C) allowed the extensive homogenization of any potential garnet growth zoning patterns. M_1/D_1 granulite facies metamorphism and deformation was complete prior to the onset of a D_2 event responsible for east-west-oriented crustal shortening and associated development of mapped thrust contacts. Non-penetrative strain was partitioned into tight east-northeast-striking folds related to D_3 deformation and late, predominantly dextral brittle faulting.

In the western study area, the oldest recognizable fabric present within metapelitic rocks of the Schooner Harbour sequence is manifest in the form of fine-grained quartz inclusion trails within core regions of garnet and andalusite poikiloblasts, commonly seen at a high-angle to S_2 . This internal fabric represents an intensification of early compositional

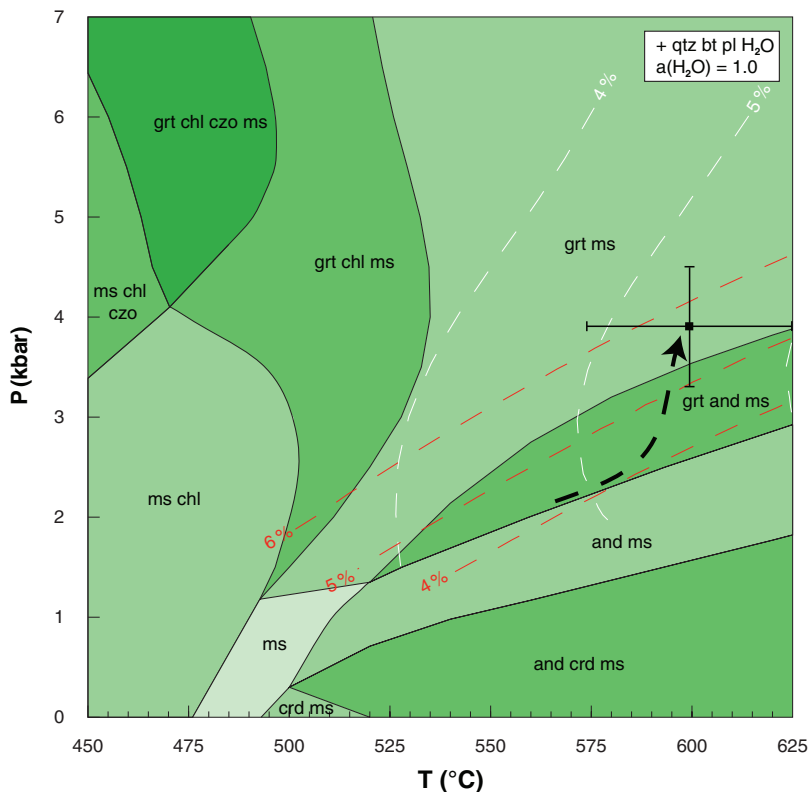


Figure 7. Pseudosection calculated in the expanded model pelite system, MnO-CaO-Na₂O-K₂O-FeO-MgO-Al₂O₃-SiO₂-H₂O (MnCNKFMASH), with THERMOCALC v.3.25 (Powell and Holland, 1988) for amphibolite-grade sample AS06-210. Pyrope and grossular isopleths (mol %) are represented by dashed white and red lines, respectively. Green-scale colour scheme reflects assemblage variance, with the darkest field having the lowest variance. The arrowed, dashed line represents a portion of the P-T path recovered from core-rim (prograde) zoning in garnet porphyroblasts (limits on garnet core composition are 4–4.2% grossular and 5–5.5% pyrope). Black cross shows average, peak P-T conditions calculated from garnet near-rim compositions (4 kbar and 600°C) and associated error margins (Fig. 6). Note, trajectory of the P-T path segment infers an anticlockwise, Buchan style (Hudson, 1980), P-T evolution. Mineral abbreviations after Kretz (1983).

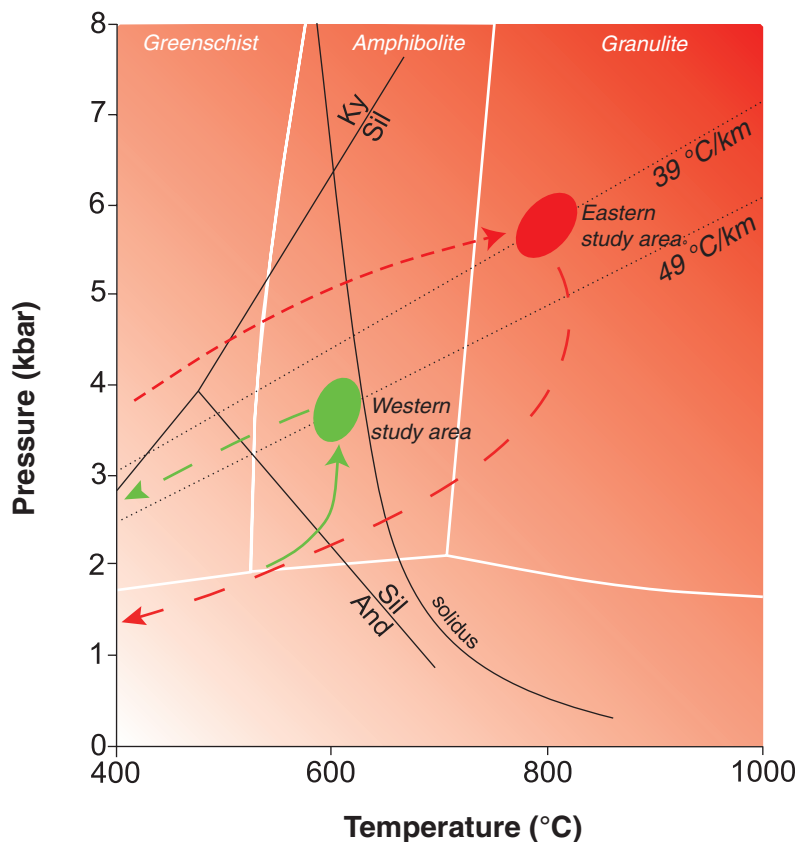


Figure 8. Pressure-Temperature paths for the eastern (red) and western (green) study areas. Dashed line segments are inferred retrograde portions of the P-T pathway. Limits of metamorphic facies (greenschist, amphibolite, and granulite) are taken from Yardley (1989). Approximate local geotherms are represented by fine-dashed lines. Note the contrasting vergence of the eastern (decompressive) and western (compressive) study area P-T paths. Aluminosilicate polymorph fields from Holdaway (1971). Solidus reaction position from Hensen and Green (1971).

layering and is denoted - $S_0 + S_1$. Porphyroblast growth of cordierite, andalusite and garnet occurred during reorientation of $S_0 + S_1$ during D_2 . Porphyroblast-matrix relations indicate that garnet growth continued in a synkinematic fashion, during pervasive fabric (S_2) development. This is consistent with a compressive P-T path segment deduced from core to near-rim (peak) garnet growth conditions in sample AS06-210 (Fig. 7), suggestive of an anticlockwise P-T pathway (Fig. 8). Poikiloblasts were rotated during this stage. D_2 is associated with north-south crustal compression, witnessed in the field area by south-vergent, east-west-striking thrust contacts (Fig. 4). Subsets of the amphibolite-facies mineral assemblage, garnet-andalusite-sillimanite-cordierite-biotite-muscovite-K-feldspar-plagioclase-quartz yield peak P-T constraints of between 2.6–3.9 kbar and 590–733°C (Fig. 6). Chemical growth zoning within garnet blasts has been partly homogenized suggesting a sustained period of high temperature and slow rates of thermal relaxation. Small, lozenge-shaped sillimanite overgrowths on the apices of peak, idioblastic andalusite poikiloblasts indicate that thermal peak conditions for M_2 reached those of the sillimanite stability field. The latest deformation event observable, D_3 , occurs post- M_2 in the form of an open crenulation of the S_2 fabric seen best at hand-sample scale and also around poikiloblasts where the micaceous fabric is significantly flattened. Late pinnitization of cordierite porphyroblasts can be ascribed to post-thermal-peak hydrothermal fluid interaction.

DISCUSSION

The potentially contrasting clockwise and anticlockwise P-T paths inferred for the supracrustal units within the eastern and western study areas, respectively (Fig. 8), imply a variance in the temporal relationship between magmatic heat supply (i.e. Cumberland batholith versus Narsajuaq arc plutons) and crustal thickening across orogenic strike. Supracrustal units from the western study area experienced a compressive P-T path, suggesting that crustal thickening (D_2) was preceded by a period of heat advection interpreted to have been associated with the emplacement of approximately 1.84 to 1.83 Ga granitic plutons of the Narsajuaq arc (Fig. 7; Rayner et al., 2008). Although a similarly elevated geotherm is implied, the eastern study area's prograde history suggests overlapping periods of crustal thickening and high-temperature metamorphism (D_1/M_1), interpreted as the cumulative result of the emplacement of the 1865 to 1848 Ma Cumberland batholith and approximately 1845 Ma accretion of the (older suite) intra-oceanic Narsajuaq arc (St-Onge et al., 2007a) yielding a clockwise P-T path (Fig. 8).

At a regional scale, results from this study illustrate that southwest Baffin Island's macroscopic thermal architecture is dominated by a progressive increase in metamorphic grade and crustal depth toward the east-northeast of the region, consistent with a more hinterland orogenic context.

P-T information from both study areas shows that an elevated geothermal gradient is required to produce the mineral assemblages and compositions observed

(39–49°C /km; Fig. 8). Assuming a perturbed continental geotherm, an increase in crustal depth of sufficient magnitude (6–7 km) across orogenic strike toward the northeast would account for granulite facies conditions in the eastern study area, compared to the amphibolite facies conditions recorded farther west on the Foxe Peninsula. Emplacement of the voluminous Cumberland batholith into Trans-Hudson Orogen's collage of upper-plate accreted units, including the Meta Incognita microcontinent (St-Onge et al., 2006) provides a temporally plausible explanation for the elevated M_1 thermal regime in the eastern study area. St-Onge et al. (2007a) and Rayner et al. (2008) constrained the M_1 event in the upper-plate of Trans-Hudson Orogen on Baffin Island to between approximately 1.85 and 1.83 Ga based on metamorphic monazite age data. Within the western study area, field relationships indicate that magmatism, likely that associated with the approximately 1.84 to 1.83 Ga suite of the Narsajuaq arc, occurred prior to the onset of D_2 thrusting. The documented crustal imbrication and associated metamorphism can be interpreted as the result of crustal shortening in the upper part of the Trans-Hudson Orogen during continent-continent collision with the lower plate Superior craton between about 1825 and 1795 Ma (St-Onge et al., 2006), thus accounting for the postulated anticlockwise P-T path (Fig. 8).

ACKNOWLEDGMENTS

Field assistance from all members of the SWBIG team is gratefully acknowledged. Helicopter transport of the highest calibre was provided by Universal Helicopters Ltd. Helpful discussions were held with Nicole Rayner, Mary Sanborn-Barrie, and Mike Young, all from GSC. Thanks also go to James Rae (University of Oxford) for friendship, encouragement and lively scientific debate. Tracy Lynds (GSC) provided invaluable cartographic support. Norman Charnley (University of Oxford) provided assistance with SEM work. A helpful and thorough review of an earlier version of this paper was provided by Natasha Wodicka (GSC).

REFERENCES

- Anderson, D.E. and Olimpio, J.C., 1977. Progressive homogenization of metamorphic garnets, south Molnar, Scotland: Evidence for volume diffusion; *Canadian Mineralogist*, v. 15, p. 205–216.
- Caddick, M.J., Bickle, M.J., Harris, N.B.W., Holland, T.J.B., Horstwood, M.S.A., Parrish, R.R., and Ahmad, T., 2007. Burial and exhumation history of a lesser Himalayan schist: Recording the formation of an inverted metamorphic sequence in NW India; *Earth and Planetary Science Letters*, v. 264, p. 375–390. doi:10.1016/j.epsl.2007.09.011
- Dunphy, J.M. and Ludden, J.N., 1998. Petrological and geochemical characteristics of a Paleoproterozoic magmatic arc (Narsajuaq Terrane, Ungava Orogen, Canada) and comparisons to Superior Province granitoids; *Precambrian Research*, v. 91, p. 109–142. doi:10.1016/S0301-9268(98)00041-2
- Fitzsimons, I.C.W. and Harley, S.L., 1994. The influence of retrograde cation exchange on granulite P-T estimates and a convergence technique for the recovery of peak metamorphic conditions; *Journal of Petrology*, v. 35, p. 543–576.
- Forbes, C.J., Betts, P.G., Weinberg, R., and Buick, I.S., 2005. A structural and metamorphic study of the Broken Hill Block, NSW, Australia; *Journal of Metamorphic Geology*, v. 23, p. 745–770. doi:10.1111/j.1525-1314.2005.00608.x
- Hensen, B.J. and Green, D.H., 1971. Experimental study of the stability of cordierite and garnet in pelitic compositions at high pressures and temperatures. I. Compositions with excess alumino-silicate; *Contributions to Mineralogy and Petrology*, v. 33, p. 309–330. doi:10.1007/BF00382571
- Hensen, B.J. and Green, D.H., 1973. Experimental study of the stability of cordierite and garnet in pelitic compositions at high pressures and temperatures. III. Synthesis of experimental data and geological applications; *Contributions to Mineralogy and Petrology*, v. 38, p. 151–166. doi:10.1007/BF00373879
- Hoffman, P.F., 1988. United Plates of America, the birth of a craton: Early Proterozoic assembly and growth of Laurentia; *Annual Review of Earth and Planetary Sciences*, v. 16, p. 543–603. doi:10.1146/annurev.ea.16.050188.002551
- Holdaway, M.J., 1971. Stability of andalusite and the aluminium silicate phase diagram; *American Journal of Science*, v. 271, p. 97–131.
- Holdaway, M.J., 2000. Application of new experimental and garnet Margules data to the garnet-biotite geothermometer; *The American Mineralogist*, v. 85, p. 881–892.
- Holdaway, M.J. and Lee, S.M., 1977. Fe-Mg cordierite stability in high-grade pelitic rocks based on experimental, theoretical, and natural observations; *Contributions to Mineralogy and Petrology*, v. 63, p. 175–198. doi:10.1007/BF00398778
- Holland, T.J.B. and Powell, R., 1995. AX activity – composition software available for download from ftp://www.esc.cam.ac.uk/pub/minp/thermocalc/.
- Holland, T.J.B. and Powell, R., 1998. An internally consistent thermodynamic data set for phases of petrological interest; *Journal of Metamorphic Geology*, v. 16, p. 309–343. doi:10.1111/j.1525-1314.1998.00140.x
- Hudson, N.F.C., 1980. Regional metamorphism of some Dalradian pelites in the Buchan area, N.E. Scotland; *Contributions to Mineralogy and Petrology*, v. 73, p. 39–51. doi:10.1007/BF00376259
- Jackson, G.D., Hunt, P.A., Loveridge, W.D., and Parrish, R.R., 1990. Reconnaissance geochronology of southern Baffin Island, N.W.T.; *Geological Survey of Canada, Paper 89-2*, p. 123–148.
- Kretz, R., 1983. Symbols for rock-forming minerals; *The American Mineralogist*, v. 68, p. 277–279.
- Lewry, J.F. and Collerson, K.D., 1990. The Trans-Hudson Orogen; extent, subdivisions, and problems; in *The Early Proterozoic Trans-Hudson Orogen of North America*, (ed.) J.F. Lewry and M.R. Stauffer; *Geological Association of Canada, Special Paper 37*, p. 1–14.

- Pattison, D.R.M., Chacko, T., Farquhar, J., and McFarlane, C.R.M., 2003. Temperatures of granulite-facies metamorphism: Constraints from experimental phase equilibria and thermobarometry corrected for retrograde exchange; *Journal of Petrology*, v. 44, p. 867–899. doi:10.1093/petrology/44.5.867
- Perchuk, L.L. and Lavrent'eva, I.V., 1983. Experimental investigation of exchange equilibrium in the system cordierite-garnet-biotite; in *Kinetics and equilibrium in mineral reactions*, (ed.) S. K. Saxena (*Advances in physical geochemistry*, v. 3.). New York, Heidelberg, Berlin: Springer-Verlag, 273 p.
- Powell, R. and Holland, T.J.B., 1988. THERMOCALC software available from: ftp://www.esc.cam.ac.uk/pub/minp/thermocalc/.
- Rayner, N., Sanborn-Barrie, M., Wodicka, N., and St-Onge, M., 2007. New U-Pb geochronological constraints on the timing of deformation and the nature of basement of SW Baffin Island, Nunavut; in *35th Annual Yellowknife Geoscience Forum Abstracts*, (comp.) S. Cairns and H. Falck; v. 49.
- Rayner, N.M., St-Onge, M.R., Berman, R.G., Sanborn-Barrie, M., and Wodicka, N., 2008. Polyphase tectonometamorphic history in the upper plate of Trans-Hudson orogen (southern Baffin Is.); *Geochimica et Cosmochimica Acta*, v. 72, p. A780 (abstract).
- Sanborn-Barrie, M., St-Onge, M.R., Young, M.D., and James, D.T., 2008. Bedrock geology of southwestern Baffin Island, Nunavut: expanding the tectonostratigraphic framework with relevance to mineral resources; *Geological Survey of Canada, Current Research 2008-6*, 16 p.
- Scott, D.J. and Wodicka, N., 1998. A second report on the U-Pb geochronology of southern Baffin Island; *Geological Survey of Canada, Paper 1998-F*, p. 47–57.
- Scott, D.J., St-Onge, M.R., Wodicka, N., and Hanmer, S., 1997. Geology of the Markham Bay – Crooks Inlet area, southern Baffin Island, Northwest Territories; *Geological Survey of Canada, Current Research 1997-C*, p. 157–166.
- Scott, D.J., Stern, R.A., St-Onge, M.R., and McMullen, S.M., 2002. U-Pb geochronology of detrital zircons in metasedimentary rocks from southern Baffin Island: implications for the Paleoproterozoic tectonic evolution of Northeastern Laurentia; *Canadian Journal of Earth Sciences*, v. 39, p. 611–623. doi:10.1139/e01-093
- Sevigny, J.H. and Ghent, E.D., 1989. Pressure, temperature and fluid composition during amphibolite facies metamorphism of graphitic metapelites, Howard Ridge, British Columbia; *Journal of Metamorphic Geology*, v. 7, p. 497–505. doi:10.1111/j.1525-1314.1989.tb00612.x
- Spear, F., 1993. *Metamorphic Phase Equilibria and P-T-t paths*; Mineralogical Society of America Monograph. p. 578–579.
- St-Onge, M.R., Wodicka, N., and Lucas, S.B., 2000. Granulite- and amphibolite-facies metamorphism in a convergent-plate margin setting: synthesis of the Quebec-Baffin segment of the Trans-Hudson Orogen; *Canadian Mineralogist*, v. 38, p. 379–398. doi:10.2113/gscanmin.38.2.379
- St-Onge, M.R., Searle, M.P., and Wodicka, N., 2006. Trans-Hudson Orogen of North America and Himalaya Karakoram-Tibetan Orogen of Asia: Structural and thermal characteristics of the lower and upper plates; *Tectonics*, v. 25, cit. no. TC4006. doi:10.1029/2005TC001907
- St-Onge, M.R., Wodicka, N., and Ijewliw, O., 2007a. Polymetamorphic evolution of the Trans-Hudson Orogen, Baffin Island, Canada: Integration of petrological, structural and geochronological data; *Journal of Petrology*, v. 48, p. 271–302. doi:10.1093/petrology/egl060
- St-Onge, M.R., Sanborn-Barrie, M., and Young, M., 2007b. Geology, Mingo Lake, Baffin Island, Nunavut; *Geological Survey of Canada Open File Map 5433*, scale 1:200 000.
- St-Onge, M.R., Sanborn-Barrie, M., and Young, M., 2007c. Geology, Foxe Peninsula, Baffin Island, Nunavut; *Geological Survey of Canada Open File Map 5434*, scale 1:200 000.
- St-Onge, M.R., van Gool, J.A.M., Garde, A.A., and Scott, D.J., in press. Correlation of Archaean and Paleoproterozoic units between northeastern Canada and western Greenland: constraining the pre-collisional upper plate accretionary history of the Trans-Hudson Orogen; *Geological Society, Special Publication – Accretionary Orogens through Space and Time*.
- Thériault, R.J., St-Onge, M.R., and Scott, D.J., 2001. Nd isotopic and geochemical signature of the Paleoproterozoic Trans-Hudson Orogen, southern Baffin Island, Canada: Implications for the evolution of eastern Laurentia; *Precambrian Research*, v. 108, p. 113–138. doi:10.1016/S0301-9268(00)00159-5
- Tinkham, D.K., Zuuaga, C.A., and Stowell, H.H., 2003. Metapelite phase equilibria modelling in MnNCKFMASH: the effect of variable Al₂O₃ and MgO/(MgO + FeO) on mineral stability; *The American Mineralogist*, v. 88, p. 1174.
- Vance, D. and Mahar, E., 1998. Pressure-temperature paths from P-T pseudosections and zoned garnets: potential limitations and examples from the Zaskar Himalaya, northwest India; *Contributions to Mineralogy and Petrology*, v. 132, p. 225–245. doi:10.1007/s004100050419
- Vernon, R.H. and Clarke, G.L., 2008. *Principles of Metamorphic Petrology*; Cambridge University Press. p. 206–252.
- Wodicka, N. and Scott, D.J., 1997. A preliminary report on the U-Pb geochronology of the Meta Incognita Peninsula, southern Baffin Island, Northwest Territories; *Geological Survey of Canada, Paper 1997-C*, p. 167–178.
- Wodicka, N., St-Onge, M.R., Sanborn-Barrie, M., Rayner, N. and James, D.T., 2008a. Basement-cover relationships in Trans-Hudson Orogen of southwest Baffin Island: constraints from SHRIMP U-Pb geochronology; *Geological Survey of Canada - Nunavut workshop abstract*.
- Wodicka, N., St-Onge, M.R., and Whalen, J.B., 2008b. Characteristics of two opposing continental margin successions in northeast Laurentia; *Geochimica et Cosmochimica Acta*, v. 72, p. A1030.
- Yardley, B., 1989. *Introduction to Metamorphic Petrology*; Longman Scientific and Technical, Harlow.
- Zuluaga, C.A., Stowell, H.H., and Tinkham, D.K., 2005. The effect of zoned garnet on metapelite pseudosection topology and calculated metamorphic P-T paths; *The American Mineralogist*, v. 90, p. 1619–1628. doi:10.2138/am.2005.1741

Geological Survey of Canada Project NM1-10083